Mathematical Modeling of Fast and Accurate Coupled Electromagnetic-Thermal Analysis

Jun-Yeol Ryu, Sung-Woo Hwang, Jun-Woo Chin, Yong-Suk Hwang, Sang Won Yoon, *Senior Member, IEEE*, and Myung-Seop Lim, *Member, IEEE*

***Abstract*—This article proposes a fast and accurate coupled electromagnetic-thermal analysis method for a permanent magnet synchronous motor. In conventional design methods, the electric and thermal characteristics are calculated simultaneously using a finite element analysis (FEA). However, FEA requires considerable computational time. Therefore, in order to reduce the computational time, mathematical models of the electric parameters and characteristics were proposed as an alternative. Accordingly, the models of the electric parameter, such as *d*- and *q*-axis inductance and flux linkage, were obtained using a modified lumped parameter magnetic circuit containing a reluctance of an iron core. Furthermore, the models were fitted according to the formula type to consider nonlinearity according to variations in current and temperature. The electric parameters calculated by FEA were used for curve fitting. A greater number of FEA points were required to determine the effect of current and temperature on the electric parameters. Curve fitting using an appropriate formula type was performed considering the accuracy and minimum number of analysis points. Mathematical modeling of the electric characteristics, including efficiency and losses, was performed. The models of losses were coupled as heat sources to the lumped parameter thermal network, which is well known for its low computational time. The proposed coupled analysis method was applied to a reference motor; through this analysis, the electric characteristics and temperature distribution were calculated simultaneously, considering changes in losses and temperature distribution. The experimental validation was conducted with an acceptable error of 4.4%.**

***Index Terms*—Coupled electromagnetic-thermal analysis, electric brake, lumped parameter magnetic circuit, lumped parameter thermal network, mathematical modeling, permanent magnet synchronous motor (PMSM).**

Manuscript received October 6, 2020; revised March 31, 2021; accepted May 24, 2021. Date of publication June 7, 2021; date of current version September 16, 2021. Paper no. 2020-EMC-1464.R1, presented at the 2020 IEEE Transportation Electrification Conference & Expo, Chicago, IL, USA, Jun. 24–26, and approved for publication in the IEEE TRANSACTIONS ON INDUSTRY APPLICATIONS by the Electric Machines Committee of the IEEE Industry Application Society. This work was supported by the National Research Foundation of Korea (NRF) grant funded by the Korea government (MSIT) under Grant NRF-2020R1A4A4079701. *(Corresponding author: Myung-Seop Lim.)*

Jun-Yeol Ryu, Sung-Woo Hwang, Jun-Woo Chin, Sang Won Yoon, and Myung-Seop Lim are with the Department of Automotive Engineering, Hanyang University, Seoul 04763, South Korea (e-mail: jesus0925@hanyang.ac.kr; supertramph@hanyang.ac.kr; cjw1254@hanyang.ac.kr; swyoon@hanyang.ac.kr; myungseop@hanyang.ac.kr).

Yong-Suk Hwang is with the MANDO Corp., Seongnam-si 13486, South Korea (e-mail: ys.hwang@halla.com).

Color versions of one or more figures in this article are available at https://doi.org/10.1109/TIA.2021.3086823.

Digital Object Identifier 10.1109/TIA.2021.3086823

I. INTRODUCTION

PERMANENT magnet synchronous motors (PMSMs) are widely used in electric brake systems owing to their high power density and efficiency [1]–[3]. Depending on the braking pattern, the brake system motor is operated under various loads and thermal conditions. Conventionally, a PMSM is designed under fixed harsh thermal conditions, which increases its possibility of being overdesigned. Furthermore, because the electric and thermal characteristics interact with each other, the electric characteristics, such as efficiency and losses, calculated under a fixed thermal condition may be incorrect.

Because the residual induction of a permanent magnet (PM) and the resistance of an armature coil vary according to temperature [4], [5], the electric characteristics also change [6]–[8]. It is difficult to accurately predict the temperature distribution if the losses are calculated at a fixed temperature. In a conventional design, a PMSM is designed either under a fixed load condition or at ambient temperature [9], [10]. In such a case, when the electric brake is operated, the actual braking performance may differ from the analysis results. As a solution to this problem, a coupled electromagnetic-thermal analysis method is essential for predicting both electric and thermal characteristics simultaneously. Accordingly, the coupled analysis method proposed herein can enable rapid calculation of the motor performance under various load and thermal conditions.

The coupled electromagnetic-thermal analysis method has been studied extensively to accurately predict the electric performance and temperature distribution. In [11], the core loss distribution of the motor part was calculated through finite-element analysis (FEA), and these losses were reflected in a lumped parameter thermal network (LPTN). Although the temperature distribution was calculated considering the exact losses, the electric characteristics for the changed temperature were not recalculated. For a coupled analysis considering both the electric and thermal variations independently, Zhang *et al*. proposed an FEA that couples the governing equations of electromagnetic and thermal fields [12]. Although the FEA according to time produces the exact trend of the electric and thermal characteristics, it requires considerable computational time. Consequently, even when electric characteristics are analyzed through a FEA under various thermal conditions, it is still time-consuming. Therefore, a coupled analysis method for motor design is required to enable both easy preprocessing and fast computation while simultaneously considering the variation in electric characteristics as well as temperature distribution with respect to time.

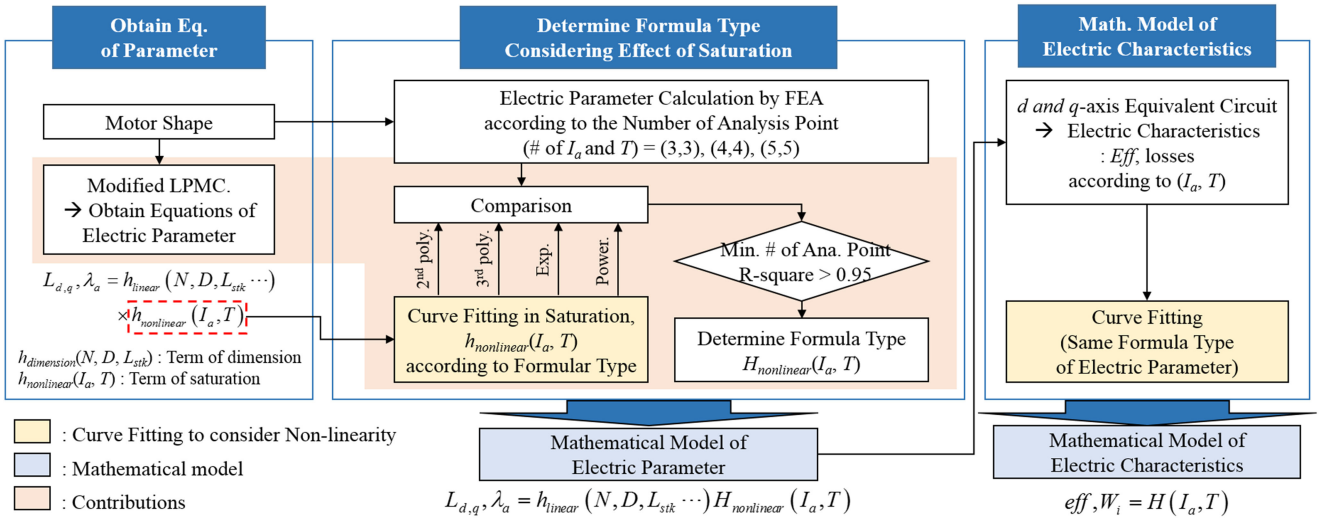

Fig. 1. Flowchart of the proposed mathematical modeling of electric parameters and characteristics.

To reduce the computational time, the electric and thermal characteristics were calculated using the mathematical models and LPTN, respectively. Studies on mathematical modeling were performed, and the models of electric parameters, such as *d*- and *q*-axis inductance and flux linkage by the PM, were obtained based on a modified lumped-parameter magnetic circuit (LPMC). In particular, reluctances of an iron core, which present a nonlinear material property, was considered in the modified LPMC. Curve fitting of the nonlinear property was performed to utilize it in the models. In addition, the models of the electric characteristics, including efficiency, copper loss, and core loss, were derived based on a *d*- and *q*-axis equivalent circuit model. By only computing a simple equation, the time required to calculate the electric characteristics was reduced. The proposed mathematical models of the losses and electric characteristics were coupled to the LPTN. Specifically, the losses calculated by the models were considered as the heat sources of the LPTN, and the efficiency was calculated considering the updated temperature computed by the LPTN. The proposed coupled analysis method was applied to a reference motor designed for an electric brake system; this coupled analysis was performed at each step. For each step, the electric and thermal characteristics were calculated considering the changes in the losses and temperature distribution in its previous step. The validity of the proposed coupled analysis method was verified through experiments, which measured the temperature distribution and torque–speed–current (T-N-I) curves. The experimental results were compared with the analysis results, and the error was found to be acceptable within 4.4%.

The contributions of this article are as follows.

1) Mathematical models enable quick calculation of the electric characteristics by computing only a simple equation.
2) The number of analysis points required to predict the temperature-dependent behaviors of electric parameters was reduced, which further reduced the time consumption.

Details of the proposed mathematical modeling and the main analysis process are presented in Sections II and III, respectively. The experimental verification is presented in Section IV.

II. Mathematical Modeling of Temperature Dependent Behavior of Electric Characteristics

The electric parameters of PMSMs need to be estimated owing to their influence on the electric characteristics. These parameters change due to current and temperature variations. In a conventional design method, the electric parameters are calculated using the FEA relative to the current under a fixed temperature distribution. Conducting the FEA to evaluate the trends in terms of current and temperature may be time-consuming. Therefore, the mathematical models of electric parameters and characteristics are suitable alternatives in coupled analysis. Fig. 1 illustrates a flowchart of the mathematical modeling of the electric parameters and characteristics. First, mathematical models of the electric parameters were derived using the modified LPMC. Because of the reluctances of air and PM in the conventional LPMC, it was difficult to predict the nonlinearity of the electric parameters using the equation, and only the parameter changes for the dimension could be predicted. The modified LPMC includes a core reluctance, which describes the nonlinearity of the saturation. Therefore, the proposed mathematical model consists of the terms of the dimension and saturation. Second, curve fitting was conducted for the nonlinear term; it was fitted according to different formula type. Subsequently, FEA results were required for curve fitting. However, further study on the temperature-dependent behavior is required for a coupled analysis. To consider the trends in temperature as well as current, more FEA points are required, which may be time-consuming. FEA was conducted to study the reliability of the model according to the number of analysis point for curve fitting. Thereafter, the appropriate formula type was determined by comparing the results of the FEA and fitted curves according to the formula types, considering that the accuracy is achievable with the minimum number of analysis points. Therefore, mathematical models of the electric parameters were accurate, and a limited number of analysis points were required for curve fitting. Following this, the electric characteristics were calculated using a *d*- and *q*-axis equivalent circuit model. The maps of the electric parameters

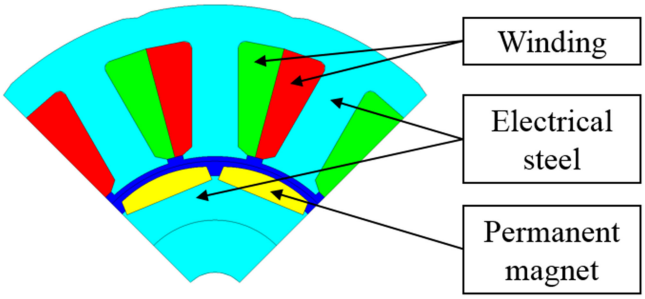

Fig. 2. Reference model designed for the electric brake system.

TABLE I
SPECIFICATIONS OF THE REFERENCE MODEL

	Value	Unit
Type	SPMSM	
Pole / slot number	8 / 12	
Stator outer diameter	86.8	mm
Stack length	34.5	mm
DC link voltage	12	V
Residual induction @ 20°C	1.345	T
Core material	27PNF1350	
Control method	$I_d = 0$ control	

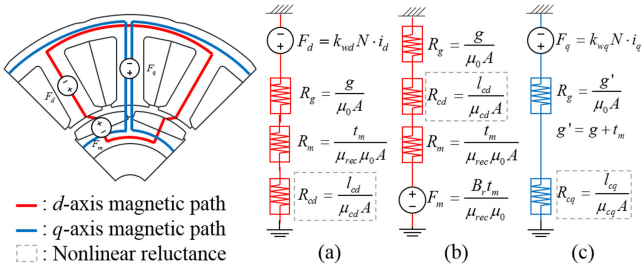

Fig. 3. d- and q-axis modified LPMC. (a) MMF is q-axis current. (b) MMF is d-axis current. (c) MMF is PM.

for these circuits were calculated using the proposed mathematical models of electric parameters. Mathematical models of the electric characteristics were fitted with the same formula type as those in the case of electric parameters. Furthermore, mathematical modeling was performed for the reference motor as illustrated in Fig. 2; detailed specifications are listed in Table I. According to the vehicular design specifications, the temperature range was set from –40 to 200 °C [13].

A. Mathematical Modeling of Electric Parameters

In conventional studies, mathematical models of the electric parameters were obtained using LPMC. Although the LPMC is one of the methods used to predict electric parameters, its nonlinearity is not considered [14], [15]. This article proposes a modified LPMC that includes the reluctance of the iron core to consider the nonlinearity, as shown in Fig. 3. In addition, three magneto-motive forces (MMFs) act on the independent d- and q-axis magnetic paths, namely the d-axis current, q-axis current, and the PM [16], [17]. In Fig. 3, the LPMCs are modeled for each MMF. In each LPMC, flux was generated by each MMF, and the reluctances of all components through which the flux passes were included. After each flux of the d- and q-axis LPMC was calculated, inductances were obtained by dividing the flux by the current in case the current was the MMF. Mathematical models of the d- and q-axis inductances and the flux linkage by the PM obtained using the proposed LPMC are expressed by (1) and (2), respectively. The residual induction of PM in (2) changes linearly with temperature, as shown in the following equation:

$$L_d,\, L_q = \frac{3}{\pi}\left(\frac{k_w N}{2P_n}\right)^2 (D \cdot L_{\text{stk}}) \times h_{\text{nonlinear}} \tag{1}$$

$$\lambda_a = \frac{3}{\pi}\left(\frac{k_w N}{2P_n}\right)(D \cdot L_{\text{stk}})\frac{B_r t_m}{\mu_{\text{rec}}\mu_0} \times h_{\text{nonlinear}} \tag{2}$$

$$B_r = B_{r@20\,^\circ\text{C}} \times [1 + \alpha \times (T - 20\,^\circ\text{C})] \tag{3}$$

$$h_{\text{nonlinear}} = \left[\frac{1}{g/\mu_0 + l_c/\mu_c}\right] \tag{4}$$

where L_d and L_q are the d- and q-axis inductances, respectively, P_n is the number of pole pairs, D is the rotor diameter, L_{stk} is the stack length, λ_a is the flux linkage by PM, g is the magnetic air gap, μ_0 is the vacuum permeability, l_c is the length of magnetic path of the iron core, μ_c is the core permeability, α is a temperature coefficient, T is a temperature, and B_r is the residual induction at an arbitrary temperature of T.

As the current increases, the nonlinearity of the inductance grows because of the iron core saturation. Similarly, residual induction of the PM varies with temperature, which causes a change in the flux generated by the PM. In addition, it affects the saturation of the iron core. Therefore, the inductance changes nonlinearly according to the current and temperature due to saturation. In the mathematical models of the d- and q-axis inductance and flux linkage by the PM, $h_{\text{nonlinear}}$ expressed by (4) represents the nonlinear behavior, which depends on the current and temperature.

To describe the nonlinear property, the electric parameters according to current were obtained through curve fitting as used in the conventional design. Although curve fitting is a suitable method for predicting nonlinear properties [18], several formula types, such as polynomial, exponential, and power series equations, have been proposed to describe the electric parameters [19]–[21]. However, these studies did not include any temperature-dependent behaviors. Therefore, to determine the formula type that can best express the behavior of electric parameters with respect to current and temperature, the curve fitting for the function $h_{\text{nonlinear}}$ in (4) was conducted according to various formula types. The standard forms of the polynomial, exponential, and power series equation are represented by the following equations:

$$h_{\text{polynomial}}(x) = ax^3 + bx^2 + cx + d \tag{5}$$

$$h_{\text{exponential}}(x) = ae^{bx} + c \tag{6}$$

$$h_{\text{power series}}(x) = ax^b + c \tag{7}$$

where a, b, c, and d are coefficients.

TABLE II
R-SQUARE ACCORDING TO FUNCTION TYPES AND NUMBER OF ANALYSIS POINTS FOR CURVE FITTING

Parameter	Function types for curve fitting	Number of analysis points				
		3	4	5	6	7
$L_{d,\,q}$	3rd polynomial	0	1	0.99	1	1
	2nd polynomial	0.99	1	0.98	0.99	1
	Exponential	0.88	0.91	0.91	0.92	0.95
	Power series			< 0.8		
λ_a	3rd polynomial	0	1	1	1	1
	2nd polynomial	1	1	1	1	1
	Exponential	0.87	0.88	0.88	0.84	0.86
	Power series			< 0.8		

Electric parameters were calculated using mathematical models whose nonlinear components were fitted according to the formula type. Finally, the calculated electric parameters were compared with the FEA results. In Table II, the *R*-square values are presented according to formula types and the number of analysis points used for curve fitting. The first-order polynomial was excluded because it could not match the nonlinearity; the *R*-square value of the exponential was low over the entire range and was therefore not suitable for describing the electric parameters. Moreover, the results of the power series were also inaccurate because the *R*-square values were low for all electric parameters. Although the results calculated by the curve fitted with a third-order polynomial resulted in high accuracy, they were insufficient because four analysis points were required for curve fitting. As an alternative to the third-order polynomial, electric parameters fitted with a second-order polynomial provided suitable accuracy with minimum number of three analysis points. Fig. 4 shows the error map of the electric parameters between the results of the FEA and the mathematical model fitted with each formula type; the number of analysis points for curve fitting was selected as three. In Fig. 4, the error map of the power series is excluded because of its low *R*-square value, as given in Table II. Using the *R*-square values and error map, it was verified that the mathematical model fitted with second-order polynomial can accurately describe the electric parameters. Accordingly, the obtained mathematical models of the electric parameters are expressed as follows:

$$L_d,\, L_q = \frac{3}{\pi}\left(\frac{k_w N}{2P_n}\right)^2 (D \cdot L_{stk}) \times \left(C_1 {I_a}^2 + C_2 I_a + C_3\right)\left(C_4 T^2 + C_5 T + C_6\right) \tag{8}$$

$$\lambda_a = \frac{3}{\pi}\left(\frac{k_w N}{2P_n}\right)(D \cdot L_{stk})\frac{B_r t_m}{\mu_{rec}\mu_0} \times \left(C_7 {I_a}^2 + C_8 I_a + C_9\right)\left(C_{10} T^2 + C_{11} T + C_{12}\right) \tag{9}$$

where C_j with $j = 1, \ldots, 12$ are undetermined coefficients, and I_a is the current.

B. Mathematical Modeling of Electric Characteristics

Electric characteristics are calculated using the *d*- and *q*-axis equivalent circuit models and voltage equations, which are represented by (10) and (11) [22]–[25]. Because the reference model is operated under the $I_d = 0$ control, the motor characteristics are monotonically changed and were dependent only the current amplitude at a certain temperature. Therefore, a mathematical model can be fitted with a simple equation according to the current amplitude and temperature. The torque thus obtained is expressed in (12). The electric parameter map used in the voltage equation was calculated using the proposed mathematical models of the electric parameters

$$\begin{bmatrix} v_d \\ v_q \end{bmatrix} = R_a \begin{bmatrix} i_{od} \\ i_{oq} \end{bmatrix} + \left(1 + \frac{R_a}{R_c}\right)\begin{bmatrix} v_{od} \\ v_{oq} \end{bmatrix} + p\begin{bmatrix} L_d & 0 \\ 0 & L_q \end{bmatrix}\begin{bmatrix} i_{od} \\ i_{oq} \end{bmatrix} \tag{10}$$

$$\begin{bmatrix} v_{od} \\ v_{oq} \end{bmatrix} = \begin{bmatrix} 0 & -\omega L_q \\ \omega L_d & 0 \end{bmatrix}\begin{bmatrix} i_{od} \\ i_{oq} \end{bmatrix} + \begin{bmatrix} 0 \\ \omega \psi_a \end{bmatrix} \tag{11}$$

$$T_e = P_n\left[\psi_a i_{oq}\right],\ \ i_{od} = 0 \tag{12}$$

where i_d and i_q are the *d*- and *q*-axis armature currents, respectively; v_d and v_q are the *d*- and *q*-axis voltages, respectively; i_{od} and i_{oq} are the currents subtracted from the *d*- and *q*-axis currents and result in the iron losses from the input currents i_d and i_q, respectively; R_a is the phase resistance of the armature winding; R_c is the equivalent resistance of the iron loss; L_d and L_q are the *d*- and *q*-axis inductances, respectively; p is the differential operator as *d*/*dt*; ψ_a is the flux linkage by the PM, T_e is a torque, and ω is the electrical speed in radians per second.

Mathematical models of the electric characteristics were fitted with the results calculated by the *d*- and *q*-axis equivalent circuit

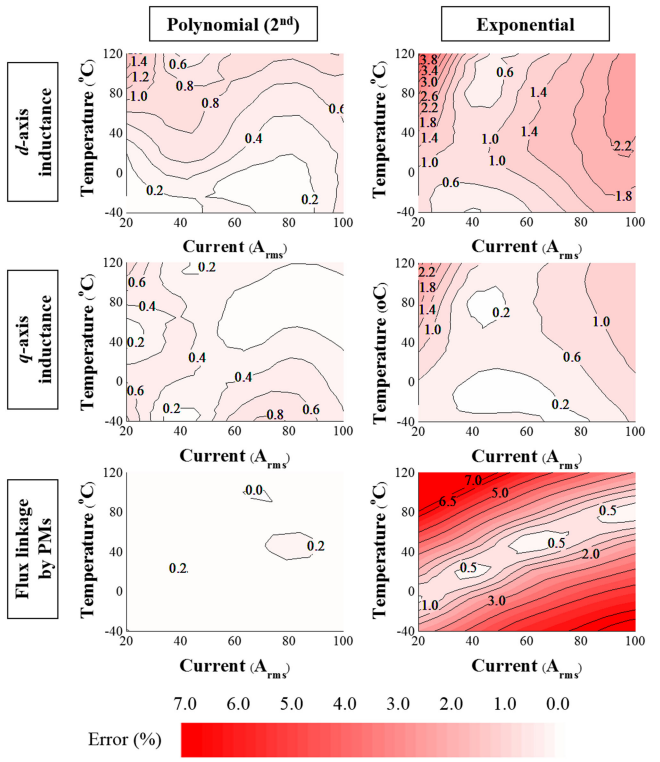

Fig. 4. Error map of electric parameters between FEA and mathematical model based on the chosen formula type.

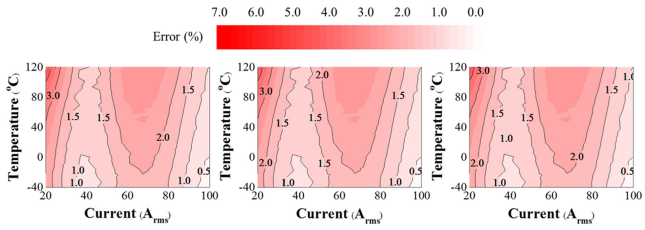

Fig. 5. Error map of core loss at different speeds. (a) 500 r/min. (b) 1000 r/min. (c) 1500 r/min.

model and voltage equation. The number of analysis points and the formula type for curve fitting were determined as three and the second-order polynomial, respectively, which is the same as in the case of mathematical modeling of the electric parameters. In the d- and q-axis equivalent circuit models, the equivalent resistance of the core loss is proportional to the square of the frequency [26]. In addition, the efficiency is affected by the core loss, which changes with the speed. Therefore, the trend according to the speed can be fitted with the second-order polynomial. Therefore, the mathematical models of efficiency and core loss are represented by (13) and (14), respectively. In addition, other electric characteristics were fitted using second-order polynomial for current and temperature. Consequently, current- and temperature-dependent behavior could be predicted using the proposed mathematical models given as follows:

$$\eta = \left(C_1 {I_a}^2 + C_2 I_a + C_3\right)\left(C_4 T^2 + C_5 T + C_6\right) \times \left(C_7 f^2 + C_8 f + C_9\right) \tag{13}$$

$$W_i = \left(C_{10} {I_a}^2 + C_{11} I_a + C_{12}\right)\left(C_{13} T^2 + C_{14} T + C_{15}\right) \times \left(C_{16} f^2 + C_{17} f + C_{18}\right) \tag{14}$$

where C_j with $j = 1, \ldots, 18$ are undetermined coefficients, η is the efficiency, f is the frequency, and W_i is the core loss.

Fig. 5 shows an error map of the core loss between the FEA results and the proposed mathematical model expressed as (14). Because it shows acceptable errors for all speeds, the proposed trend for speed was verified. Fig. 6 shows a comparison of the electric characteristics of the two-dimensional FEA and the proposed models. The trends of the electric characteristics and losses according to the current and temperature can be explained by variations in the residual induction of PM, flux of the field or armature, and saturation as mentioned in [27], [28]. Fig. 6(a) shows the copper loss map. Furthermore, as the temperature increased, the resistance of the armature coil increased. Because the copper loss is defined as the product of the square of the current and the resistance, the copper loss is proportional to the current and temperature. Second, Fig. 6(b) shows the core loss trends. Because the core loss is determined by the flux generated by the armature current, it is proportional to the current. However, the trend according to the temperature is the opposite. The flux generated by the PM decreases with increasing temperature because of the reduction in the residual induction of PM. Therefore, the efficiency and power factor are

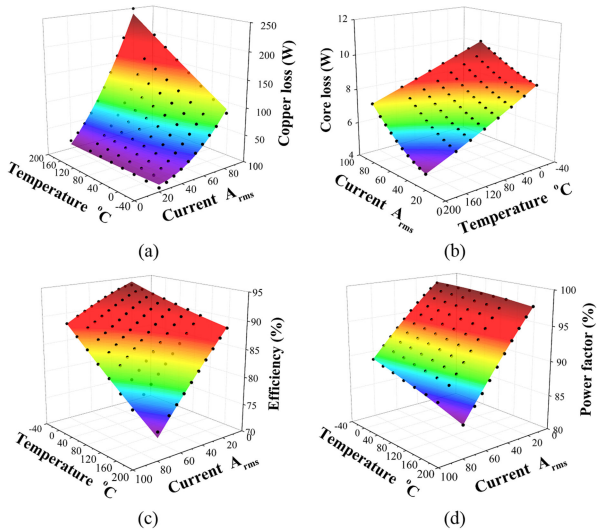

Fig. 6. Comparison of characteristics between FEA and the mathematical models. (Dot: results by the FEA, surface: results by the mathematical models.) (a) Copper loss. (b) Core loss. (c) Efficiency. (d) Power factor.

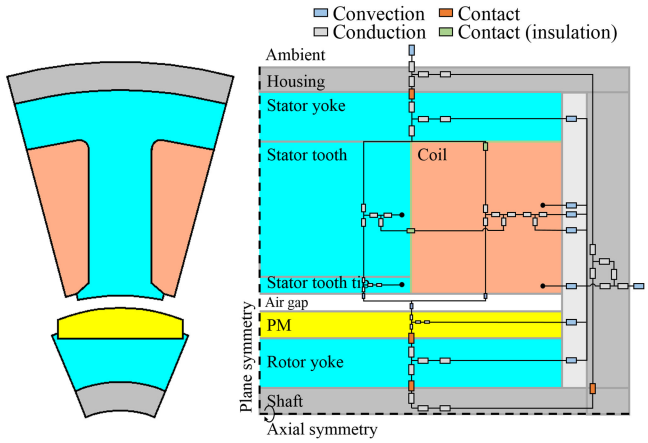

Fig. 7. LPTN of the reference model.

determined based on these losses. Although the trends of copper and core losses with respect to temperature were found to be opposite, the variation in copper loss was larger than that of core loss. Consequently, the efficiency decreased with increasing temperature. The maximum error is within 1%. Therefore, the proposed mathematical models can be used to describe the electric characteristics and losses.

C. LPTN Model and Electromagnetic-Thermal Coupling

To analyze the thermal characteristics of the reference model, a thermal analysis was conducted using the LPTN model as shown in Fig. 7 [29], [30]. The LPTN consists of the frame, end cover, stator core, coil, rotor core, PM, and shaft, all of which transfer heat by conduction, including the air gap and end space of air between the end cover and motor, which transfers heat by convection. The thermal coefficients of the LPTN are presented in Table III. The heat sources of the LPTN are copper

TABLE III
THERMAL COEFFICIENTS

Classification	Location	Dependent on	Values	Ranges
Convective heat Transfer coefficient	Environment	Cooling method, dimension, state of flow	5.1 (radial), 6.5 (axial)	5-50 [31], [32]
	Air gap	Rotation speed, state of air flow	120 @ 500rpm	5-300 [33]
	Rotor end	Rotation speed, state of air flow	38.4 @ 500rpm	5-300 [33]
	Stator end	Cooling type, rotation speed, state of air flow	15.5	15.5-300 [33], [34]
Contact conductance	Housing – stator	Contact state, material, pressure	6000	500-6000 [35], [36]
Thermal conductivity	Coil	Contact state, impregnated method, existence of varnish, material, pressure	2.4	0.5-3 [36], [37]

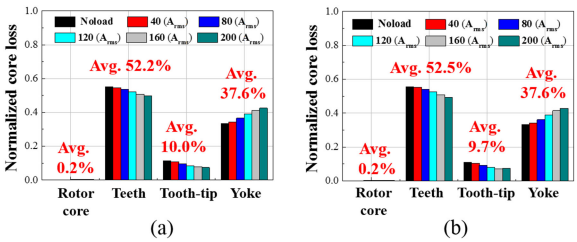

Fig. 8. Core loss distribution according to current at (a) the lowest temperature of –40 °C, and (b) the highest temperature of 200 °C.

and core losses. The resistance can be calculated using the dimensions of an armature coil with copper losses divided into components, namely the coil side and end coil. Core loss is calculated using its mathematical model, which is affected by saturation. Furthermore, the saturation of each part varies with the temperature [38]. Core loss distribution relative to thermal conditions is required to couple the core loss to each part of the LPTN. Fig. 8 shows the core loss distribution according to the current at the lowest and highest temperatures. The core loss is divided into four components: a stator yoke, stator teeth, stator tooth tip, and rotor core. The ratios of core loss distribution at the lowest and highest temperatures were similar regardless of the current. Thus, it can be stated that the core loss distribution ratio is independent of temperature. Therefore, preprocessing is simplified without estimating the core loss distribution under all load and thermal conditions.

III. MAIN PROCESS OF THE COUPLED ANALYSIS

Fig. 9 illustrates the main process of the proposed coupled electromagnetic-thermal analysis. The process of coupled analysis consists of two parts: the preprocess (PP1–PP4) and the main coupled analysis process (CA1–CA3).

PP1) Electric parameters and ratio of core loss distribution calculation by FEA.
PP2) Mathematical modeling of electric parameters.
PP3) Mathematical modeling of electric characteristics.
PP4) Electromagnetic-thermal coupling: Mathematical models of losses are coupled to the LPTN as heat sources.
CA1) Input: ambient temperature and the load condition, i.e., torque and the speed relative to time.
CA2) Calculation of electric characteristics and losses using the mathematical models.
CA3) Calculation of temperature distribution using the LPTN. The temperature was updated as it changed.

From the studies of mathematical modeling in Section II, the following conclusions were drawn from the coupled analysis. First, when the electric parameters and characteristics are fitted, the formula type determined is the second-order polynomial. Second, the number of analysis points was limited to three. Third, the core loss distribution is constant relative to the current and temperature. The detailed process of the coupled analysis is as follows.

Before the main coupled analysis, a preprocessing step was performed to simplify the process. The electric parameters were calculated by FEA relative to current and temperature, and the minimum number of analysis points according to current and temperature was determined to be three. During the calculation, the ratio of the core loss distribution was calculated at an arbitrary analysis point for the electromagnetic-thermal coupling. The mathematical models of the electric parameters were derived based on the modified LPMC. In the proposed model, the nonlinear term relative to the current and temperature was modeled as the second-order polynomial. The coefficients to consider nonlinearity were obtained by curve fitting with the results of FEA. Maps of the electric parameters were calculated using the proposed mathematical model and were reflected in the *d*- and *q*-axis equivalent circuit models to calculate the electric characteristics. Furthermore, mathematical models of the electric characteristics were fitted with the same formula type as in the case of the electric parameters. These mathematical models were coupled to the LPTN model. In this coupling, the copper loss was reflected to the armature coil part in the LPTN model, and the core loss calculated using the proposed model was multiplied by the ratio of the core loss distribution and coupled to each part of the LPTN model.

The inputs to the coupled analysis were the ambient temperature and load conditions of the load torque and speed relative to time. The initial temperatures of each part of the LPTN were set to the ambient temperature. First, the copper and core losses, which act as heat sources for the input ambient temperature and load condition, were calculated using the proposed mathematical models. Moreover, the temperature distribution was calculated using the LPTN model. Subsequently, the time and temperature of each part were updated [39]. In the next step, the electric characteristics and losses for the updated temperature and load conditions were calculated using the mathematical models. These losses considering the updated temperature were reflected again in the LPTN model, and the analysis was repeated.

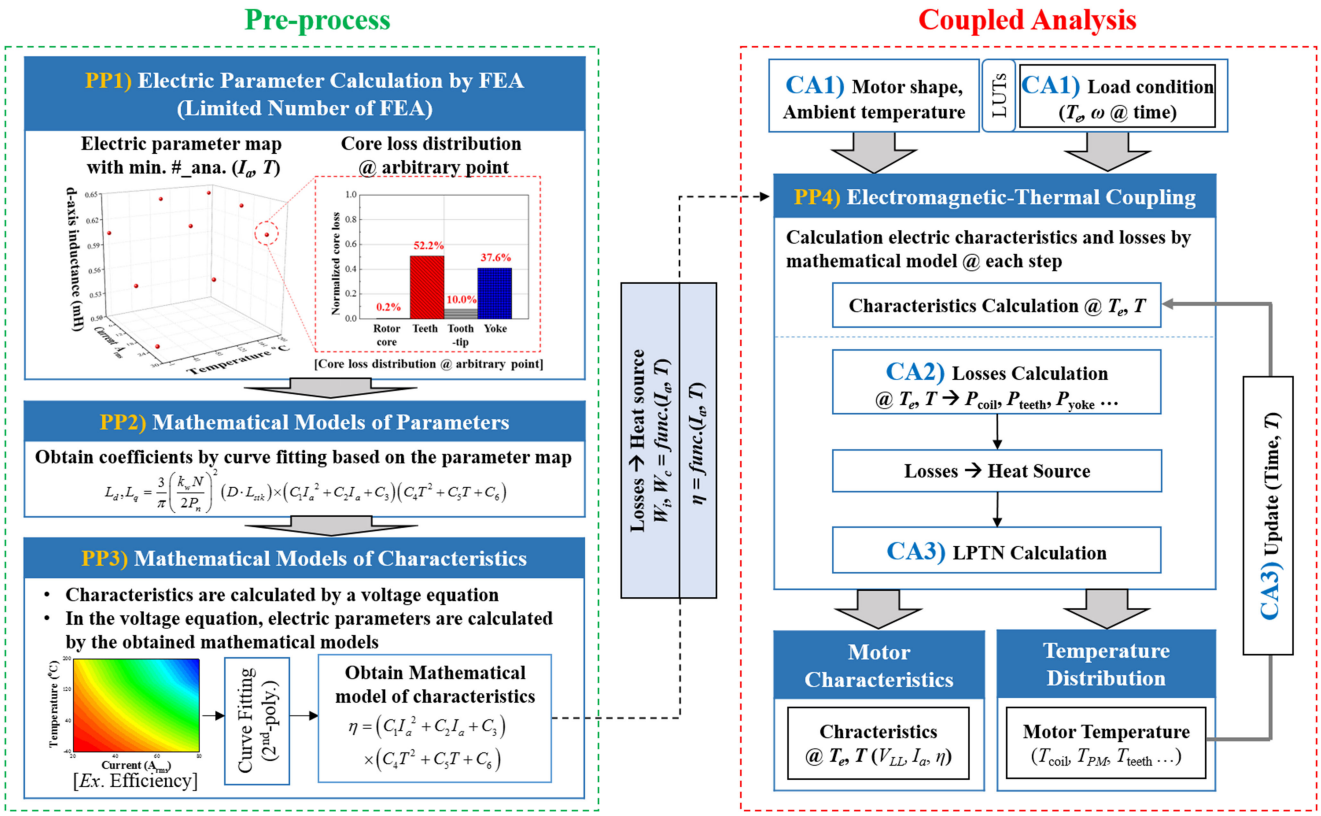

Fig. 9. Process of the coupled electromagnetic-thermal analysis.

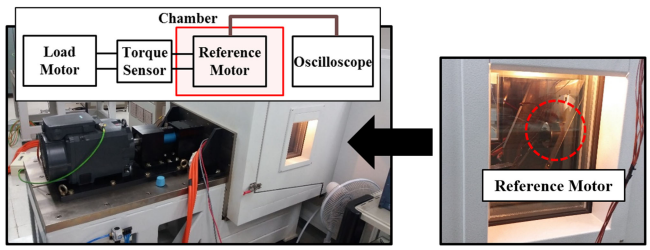

Fig. 10. Experimental setup.

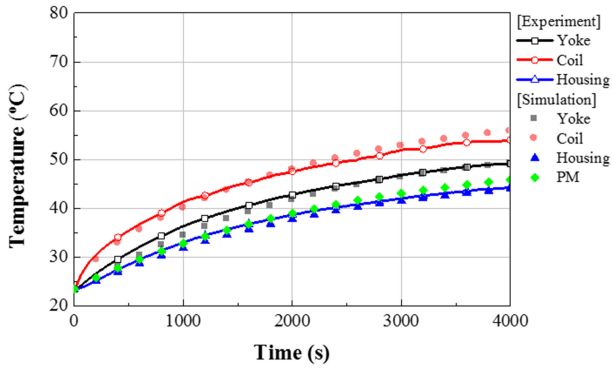

Fig. 11. Temperature saturation experiment under 1.0 N·m load condition (dot: the result predicted by the coupled analysis, solid line: the experimental result).

IV. Experimental Verification

To validate the proposed coupled electromagnetic-thermal analysis method, an experimental verification was conducted using a reference motor designed for an electric brake system. Fig. 10 illustrates the experimental setup. The reference and load motors were connected by a torque sensor used to measure the load torque. The reference motor was also connected to an oscilloscope to measure the input current and voltage. During the experiment, the speed of the load motor was maintained constant. The input current of the reference motor was controlled by measuring the load torque. The reference motor was mounted in a temperature chamber to maintain a constant ambient temperature. The temperature distribution of the reference model was measured using thermocouples attached to the middle of the coil side, end coil, stator yoke, and housing. Two temperature saturation experiments were performed with a load torque of 1.0 and 1.5 N·m and with the ambient temperature and rotating speed fixed at 23.5 °C and 500 r/min, respectively.

A. Temperature Saturation Experiment

Fig. 11 presents a comparison of the temperatures obtained using the proposed coupled analysis and the experiment at load condition 1 (load torque: 1.0 N·m; speed: 500 r/min). The dots and solid lines represent the temperatures of the coupled analysis and the experiment, respectively. Table IV presents the experimental verification of electric performance. The input currents used in the proposed coupled analysis and in the experiment were

TABLE IV
PERFORMANCE COMPARISON AT LOAD CONDITION 1

	Proposed-method results	Experiment results
Ambient temperature	23.5 °C	
Load torque	1.0 Nm	
Speed	500 rpm	
Current	17.4 A_{rms}	17.2 A_{rms}
Current phase angle	0°	0°
Predicted temperature value of PM	45.8 °C	47.3 °C

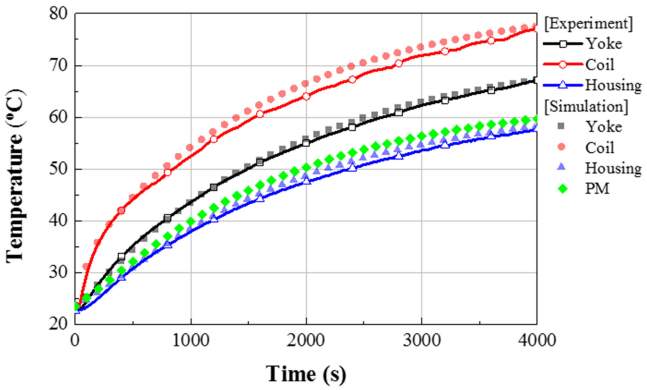

Fig. 12. Temperature saturation experiment under 1.5 N·m load condition (dot: the result predicted by the coupled analysis, solid line: the experimental result).

TABLE V
PERFORMANCE COMPARISON AT LOAD CONDITION 2

	Proposed-method results	Experiment results
Ambient temperature	23.5 °C	
Load torque	1.5 Nm	
Speed	500 rpm	
Current	27.9 A_{rms}	26.8 A_{rms}
Current phase angle	0°	0°
Predicted temperature value of PM	60.1 °C	62.9 °C

17.4 and 17.2 A_{rms}, respectively, and show an error of 1.2%. Because it is difficult to attach the thermocouple to the rotor, the temperature of the PM is indirectly predicted based on the FEA. The current measured in the experiment was considered the input of the FEA, and the residual induction that satisfied the load torque was determined through FEA. The predicted temperature values of PM obtained using the proposed coupled analysis and experiment were 45.8 and 47.3 °C, respectively, and the error was 3.2%. Similarly, Fig. 12 shows the comparison of the temperatures under load condition 2 (load torque: 1.5 N·m; speed: 500 r/min). Table V presents the experimental verification of the electric performance under the load conditions. The input current using the proposed coupled analysis and the experiment were 27.9 and 26.8 A_{rms}, respectively, and it resulted in an error of 4.1%. The predicted temperature values of PM using the proposed coupled analysis and the experiment were 60.1 and 62.9 °C, respectively, and its error was 4.4%. Therefore, the electric characteristics and temperature distribution using the proposed coupled electromagnetic-thermal analysis revealed an appropriate correlation with the experimental results.

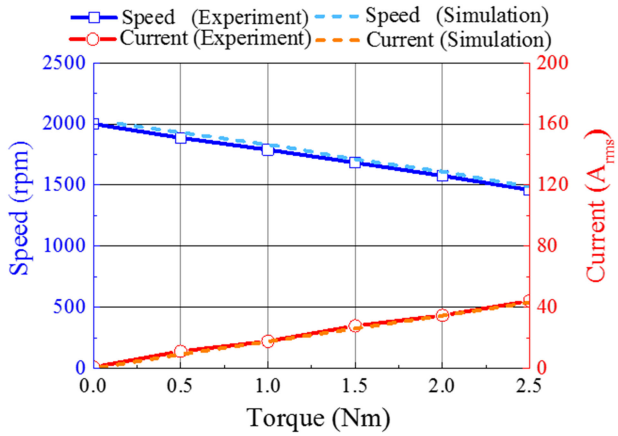

Fig. 13. T-N-I curve comparison. (Symbolic line: the experiment results, dashed line: the predicted result by the coupled analysis).

B. Electric Performance Verification

The T-N-I curve is one of the methods used to predict the electric performance of a PMSM. Fig. 13 shows the experimental verification of the electric performance. Symbolic lines indicate experimental results. The dashed lines represent the predicted results obtained using the proposed coupled analysis method. The speed and input current at each load torque were compared. Based on these experimental verifications, the proposed coupled electromagnetic-thermal analysis method could accurately calculate the electric performance and temperature distribution of the PMSM.

V. CONCLUSION

In this article, a fast and accurate coupled electromagnetic-thermal analysis method for a PMSM is proposed. Mathematical models of the electric characteristics and LPTN model were used for fast computation. First, the mathematical models of the electric parameters were obtained using the modified LPMC model. To consider the temperature-dependent nonlinearity of these parameters, the nonlinear term in the mathematical model was fitted according to the formula type. In the curve fitting, the formula type was selected as the second-order polynomial considering both the accuracy and minimum number of FEA points. Furthermore, maps of electric parameters calculated by the mathematical models were used in the *d*- and *q*-axis equivalent circuit models and in the voltage equation to calculate the electric characteristics. Mathematical models of the electric characteristics were fitted using the same formula type as that utilized in the case of electric parameters. The mathematical models of the losses were coupled to the LPTN model as a heat source. Subsequently, the proposed coupled analysis was applied to a reference model designed for an electric brake. The variations in the electric and thermal characteristics over time were calculated. This was followed by experimental verification. The error thus obtained was considered acceptable, thereby

confirming the reliability of the proposed coupled analysis. Therefore, by computing only a simple equation and using an LPTN model, the electric and thermal characteristics of a PMSM can be rapidly calculated under various load and thermal conditions. The proposed coupled analysis method can be used to accurately predict the electric and thermal characteristics by considering any operating pattern of the electric brake system. Such predictions, therefore, allow higher braking control.

REFERENCES

[1] J. Ryu, S. Hwang, J. Chin, Y. Jung, Y. Hwang, and M. Lim, "Design of PMSM by using fast and accurate stepwise coupled analysis," in *Proc. IEEE Transp. Electrific. Conf. Expo*, 2020, pp. 686–690.

[2] W. Li, X. Zhu, and J. Ju, "Hierarchical braking torque control of in-wheel-motor-driven electric vehicles over CAN," *IEEE Access*, vol. 6, pp. 65189–65198, 2018.

[3] K. Hwang and B. Kwon, "Design of low-cost BLAC motors for integrated electric brake systems," *IEEE Access*, vol. 7, pp. 184183–184193, 2019.

[4] T. Sebastian, "Temperature effects on torque production and efficiency of PM motors using NdFeB magnets," *IEEE Trans. Ind. Appl.*, vol. 31, no. 2, pp. 353–357, Mar./Apr. 1995.

[5] B. Lee, J. Jung, and J. Hong, "An improved analysis method of irreversible demagnetization for a single-phase line-start permanent magnet motor," *IEEE Trans. Magn.*, vol. 54, no. 11, Nov. 2018, Art. no. 8206905.

[6] D. Park and K. Kim, "Characteristic analysis due to temperature rise of the interior permanent magnet synchronous motor," in *Proc. IEEE Conf. Electromagn. Field Computation*, 2016, pp. 1.

[7] C. Shumei, X. Yong, Z. Tianxu, H. Shouliang, and Z. Wei, "Research on low-temperature characteristics of the motor applied in electric vehicles," in *Proc. IEEE Conf. Expo Transp. Electrific. Asia-Pac.*, 2014, pp. 1–5.

[8] Z. Zhang, G. Li, Z. Qian, Q. Ye, and Y. Xia, "Research on effect of temperature on performance and temperature compensation of interior permanent magnet motor," in *Proc. IEEE 11th Conf. Ind. Electron. Appl.*, 2016, pp. 411–414.

[9] M. Lim and J. Hong, "Design of high efficiency wound field synchronous machine with winding connection change method," *IEEE Trans. Energy Convers.*, vol. 33, no. 4, pp. 1978–1987, Dec. 2018.

[10] D. Hong, D. Joo, J. Lee, B. Woo, K. Kim, and J. Hong, "Development of a large diameter motor for turret application," *IEEE Trans. Magn.*, vol. 49, no. 5, pp. 2327–2330, May 2013.

[11] H. Yeo, H. Park, J. Seo, S. Jung, J. Ro, and H. Jung, "Electromagnetic and thermal analysis of a surface-mounted permanent-magnet motor with overhang structure," *IEEE Trans. Magn.*, vol. 53, no. 6, Jun. 2017, Art. no. 8203304.

[12] Y. Zhang, J. Ruan, T. Huang, X. Yang, H. Zhu, and G. Yang, "Calculation of temperature rise in air-cooled induction motors through 3-D coupled electromagnetic fluid-dynamical and thermal finite-element analysis," *IEEE Trans. Magn.*, vol. 48, no. 2, pp. 1047–1050, Feb. 2012.

[13] D. Kim, D. H. Kang, C. Kim, J. Kim, Y. Kim, and S. Jung, "Operation characteristic of ipmsm considering PM saturation temperature," *IEEE Trans. Appl. Supercond.*, vol. 30, no. 4, Jun. 2020, Art. no. 5207204.

[14] R. Ni, D. Xu, G. Wang, L. Ding, G. Zhang, and L. Qu, "Maximum efficiency per ampere control of permanent-magnet synchronous machines," *IEEE Trans. Ind. Electron.*, vol. 62, no. 4, pp. 2135–2143, Apr. 2015.

[15] H. Kim, J. Jeong, M. Yoon, J. Moon, and J. Hong, "Simple size determination of permanent-magnet synchronous machines," *IEEE Trans. Ind. Electron.*, vol. 64, no. 10, pp. 7972–7983, Oct. 2017.

[16] J. R. Hendershot, Jr., *Design of Brushless Permanent-Magnet Machines*. Venice, FL, USA: Motor Design Books LLC, 2010, pp. 248–261.

[17] L. Dang, N. Bernard, N. Bracikowski, and G. Berthiau, "Analytical model and reluctance network for high-speed PMSM design optimization application to electric vehicles," in *Proc. XXII Int. Conf. Elect. Mach.*, 2016, pp. 1359–1365.

[18] Z. Jian, W. Xuhui, W. Youlong, and L. Wenshan, "Modeling and analysis of nonlinear interior permanent magnet synchronous motors considering saturation and cross-magnetization effects," in *Proc. IEEE Transp. Electrif. Conf. Expo , Asia-Pac.*, 2016, pp. 611–615.

[19] H. Gurleyen and E. Mese, "A nonlinear q-Axis inductance modeling of a 12-Slot 10-pole IPM using approximate analytical methods," *IEEE Trans. Energy Convers.*, vol. 35, no. 2, pp. 621–630, Jun. 2020.

[20] A. R. Sobbouhi and A. Vahedi, "Online synchronous generator out-of-step prediction by electrical power curve fitting," *IET Gener., Transmiss. Distrib.*, vol. 14, no. 7, pp. 1169–1176, 2020.

[21] H. Gurleyen, E. Mese, J. H. Kim, and B. Sarlioglu, "Nonlinear analytical model of an inductance considering saturation and temperature variation," in *Proc. IEEE Energy Convers. Congr. Expo.*, 2017, pp. 3150–3154.

[22] G. Boztas and O. Aydogmus, "Design of a high-speed PMSM for flywheel systems," in *Proc. 4th Int. Conf. Power Electron. Appl.* , 2019, pp. 1–5.

[23] C. Dutta and S. M. Tripathi, "Comparison between conventional and loss d-q model of PMSM," in *Proc. Int. Conf. Emerg. Trends Elect. Electron. Sustain. Energy Syst.*, 2016, pp. 256–260.

[24] D. Kim, J. Lee, A. Ko, C. Won, and Y. Kim, "Braking torque control method of IPMSM for electric vehicle using 2D look-up table," in *Proc. IEEE Int. Symp. Ind. Electron.*, 2013, pp. 1–5.

[25] B. Lee, S. Kwon, T. Sun, J. Hong, G. Lee, and J. Hur, "Modeling of core loss resistance for d-q equivalent circuit analysis of IPMSM considering harmonic linkage flux," *IEEE Trans. Magn.*, vol. 47, no. 5, pp. 1066–1069, May 2011.

[26] K. Yamazaki, "Torque and efficiency calculation of an interior permanent magnet motor considering harmonic iron losses of both the stator and rotor," *IEEE Trans. Magn.*, vol. 39, no. 3, pp. 1460–1463, May 2003.

[27] A. M. Aljehaimi and P. Pillay, "Novel flux linkage estimation algorithm for a variable flux PMSM," *IEEE Trans. Ind. Appl.*, vol. 54, no. 3, pp. 2319–2335, May/Jun. 2018.

[28] S. Xiao and A. Griffo, "PWM-based flux linkage and rotor temperature estimations for permanent magnet synchronous machines," *IEEE Trans. Power Electron.*, vol. 35, no. 6, pp. 6061–6069, Jun. 2020.

[29] S. Hwang, J. Chin, and M. Lim, "Design process and verification of SPMSM for a wearable robot considering thermal characteristics through LPTN," *IEEE/ASME Trans. Mechatronics*, vol. 26, no. 2, pp. 1033–1042, Apr. 2021.

[30] J. W. Chin, K. S. Cha, M. R. Park, S. H. Park, E. C. Lee, and M. S. Lim, "High efficiency PMSM with high slot fill factor coil for heavy-duty EV traction considering AC resistance," *IEEE Trans. Energy Convers.*, vol. 36, no. 2, pp. 883–894, 2021.

[31] Y. A. Cengel and A. J. Ghajar, *Heat and Mass Transfer, Fundamentals and Applications*, 5th ed. New York, NY, USA: McGraw-Hill, 2015.

[32] D. Staton, A. Boglietti, and A. Cavagnino, "Solving the more difficult aspects of electric motor thermal analysis in small and medium size industrial induction motors," *IEEE Trans. Energy Convers.*, vol. 20, no. 3, pp. 620–628, Sep. 2005.

[33] D. A. Howey, P. R. N. Childs, and A. S. Holmes, "Air-gap convection in rotating electrical machines," *IEEE Trans. Ind. Electron.*, vol. 59, no. 3, pp. 1367–1375, Mar. 2012.

[34] P. H. Mellor, D. Roberts, and D. R. Turner, "Lumped parameter thermal model for electrical machines of TEFC design," *IEEE Proc. B Elect. Power Appl.*, vol. 138, no. 5, pp. 205–218, 1991.

[35] R. Camilleri, D. A. Howey, and M. D. McCulloch, "Experimental investigation of the thermal contact resistance in shrink fit assemblies with relevance to electrical machines," in *Proc. IET Int. Conf. Pow. Electn. Mach. Drives*, 2014, Art. no. 14251058.

[36] A. Boglietti, A. Cavagnino, and D. Staton, "Determination of critical parameters in electrical machine thermal models," *IEEE Trans. Ind. Appl.*, vol. 44, no. 4, pp. 1150–1159, Jul./Aug. 2008.

[37] N. Simpson, R. Wrobel, and P. H. Mellor, "Estimation of equivalent thermal parameters of impregnated electrical windings," *IEEE Trans. Ind. Appl.*, vol. 49, no. 6, pp. 2505–2515, Nov./Dec. 2013.

[38] S. Hwang, M. Lim, and J. Hong, "Hysteresis torque estimation method based on iron-loss analysis for permanent magnet synchronous motor," *IEEE Trans. Magn.*, vol. 52, no. 7, Jul. 2016, Art. no. 8204904.

[39] Y. Chen, X. Zhu, L. Quan, and L. Wang, "Performance analysis of a double-salient permanent-magnet double-rotor motor using electromagnetic–thermal coupling method," *IEEE Trans. Appl. Supercond.*, vol. 26, no. 4, Jun. 2016, Art. no. 5205305.

Jun-Yeol Ryu received the bachelor's degree in mechanical engineering and electronic systems engineering from Hanyang University, Ansan, South Korea, in 2016. He is currently working toward the Ph.D. degree in automotive engineering with Hanyang University, Seoul, South Korea.

His research interests include design and optimization of electric machines and analysis of electromagnetic field.

Sung-Woo Hwang received the bachelor's degree in mechanical engineering from Hanyang University, Seoul, South Korea, in 2013. He is currently working toward the Ph.D. degree in automotive engineering from Hanyang University. His research interests include practical approaches to electric machine design for automotive and robot applications.

Jun-Woo Chin received the bachelor's degree in mechanical engineering from Hanyang University, Seoul, South Korea, in 2014. He is currently working toward the Ph.D. degree in automotive engineering from Hanyang University, Seoul, South Korea.

His research interests include design, losses and multi-physics analysis of electric machines for mechatronics systems such as automotive application.

Yong-Suk Hwang received the Ph.D. degree in automotive engineering from Hanyang University, Seoul, South Korea, in 2020.

Since 2003, he has been working with MANDO. He has developed electronic controlled brake systems, traction motor for EV and electric drive for e-Cargo bike. His research interests include the development of analysis methods for effective design of electric machines.

Sang Won Yoon (Senior Member, IEEE) received the B.S. degree in electrical engineering from Seoul National University, Seoul, South Korea, in 2000, and the M.S. and Ph.D. degrees in electrical engineering and computer science from the University of Michigan, Ann Arbor, MI, USA, in 2003 and 2009, respectively.

From 2009 to 2013, he was a Senior Scientist and a Staff Researcher with the Toyota Research Institute of North America, Ann Arbor, MI, USA, where he conducted research in power electronics and sensor systems for automobiles. Since 2013, he has been with the Department of Automotive Engineering, Hanyang University, Seoul, where he is currently an Associate Professor. His current research interests include power electronics, sensors and sensor systems, electronic reliability, and their applications in conventional and future vehicle.

Myung-Seop Lim (Member, IEEE) received the bachelor's degree in mechanical engineering from Hanyang University, Seoul, South Korea, in 2012. Also, he received the master's and Ph.D. degrees in automotive engineering from the same university, in 2014 and 2017, respectively.

From 2017 to 2018, he was a Research Engineer in Hyundai Mobis, Yongin, South Korea. From 2018 to 2019, he was an Assistant Professor in Yeungnam University, Daegu, South Korea. Since 2019, he has been with Hanyang University, Seoul, South Korea, where he is currently an Assistant Professor. His research interests include electromagnetic field analysis and multi-physics analysis of electric machinery for mechatronics systems such as automotive and robot applications.